NACA RM L55L29

NACA

# RESEARCH MEMORANDUM

## RESULTS OF ROCKET MODEL TEST OF AN AIRPLANE CONFIGURATION HAVING AN ARROW WING AND SLENDER FLAT-SIDED FUSELAGE

## LIFT, DRAG, LONGITUDINAL STABILITY, LATERAL FORCE, AND JET EFFECTS AT MACH NUMBERS BETWEEN 1.0 AND 2.3

By Robert F. Peck

Langley Aeronautical Laboratory
Langley Field, Va.



NATIONAL ADVISORY COMMITTEE
FOR AERONAUTICS

WASHINGTON

February 21, 1956

NACA RM L55L29



NATIONAL ADVISORY COMMITTEE FOR AERONAUTICS

RESEARCH MEMORANDUM

# RESULTS OF ROCKET MODEL TEST OF AN AIRPLANE CONFIGURATION HAVING AN ARROW WING AND SLENDER FLAT-SIDED FUSELAGE

## LIFT, DRAG, LONGITUDINAL STABILITY, LATERAL FORCE, AND JET EFFECTS AT MACH NUMBERS BETWEEN 1.0 AND 2.3

By Robert F. Peck

## SUMMARY

A rocket-propelled model of an airplane configuration having an arrow wing with 55° leading-edge sweep and a flat-sided fuselage mounting swept horizontal and vertical tails has been tested through use of the pulsed-control technique at Mach numbers between 1.0 and 2.3. Results are presented from an investigation of longitudinal trim, lift, stability, drag, lateral force, thrust, and jet effects.

Data were, in general, obtained through the pulsed-control technique wherein the model response to a square-wave variation of control incidence is studied.

Lift and stability data agreed well with theoretical estimates. Jet-effects data were in agreement with expectations based on previous data.

## INTRODUCTION

Rocket-propelled research models equipped with variable-incidence horizontal tails are being used by the Langley Pilotless Aircraft Research Division to investigate the aerodynamic characteristics of various wings in combination with fuselage-tail configurations at high Reynolds numbers and in free flight. References 1, 2, and 3 are among several reports written in connection with this general program. Data from these models are obtained from telemetered records of the response of the models to square-wave variation of horizontal-tail incidence.

Data presented herein were obtained from a model having an arrow wing with 55° leading-edge sweep and an NACA 65A003 airfoil section and a rather slender, flat-sided fuselage mounting swept vertical and horizontal tails. This model was approximately twice as large as the models in the aforementioned references and unlike those models was equipped with a sustainer rocket (rocket contained within the model).

The Mach number range of the present test was about 1.0 to 2.3 and the Reynolds number range, $6 \times 10^6$ to $34 \times 10^6$.

## SYMBOLS

$A_L$ longitudinal accelerometer reading, g units

$A_N$ normal accelerometer reading, g units

$A_T$ transverse accelerometer reading, g units

$b$ wing span, ft

$\bar{c}$ wing mean aerodynamic chord, ft

$C_C$ chordwise force coefficient, $-A_{L_{cg}} \frac{W/S}{q}$

$C_D$ drag coefficient, $C_C \cos \alpha + C_N \sin \alpha$

$C_L$ lift coefficient, $C_N \cos \alpha - C_C \sin \alpha$

$C_m$ pitching-moment coefficient about $0.24\bar{c}$

$C_N$ normal-force coefficient, $A_{N_{cg}} \frac{W/S}{q}$

$C_Y$ lateral-force coefficient, $A_{T_{cg}} \frac{W/S}{q}$

$D$ diameter of circle with same area as maximum frontal area of fuselage, ft

$g$ acceleration due to gravity, ft/sec$^2$

$I_X$ moment of inertia in roll, slug-ft$^2$

$I_{XZ}$ product of inertia, slug-ft$^2$

$I_Y$ moment of inertia in pitch, slug-ft$^2$

$I_Z$ moment of inertia in yaw, slug-ft$^2$

M Mach number

p free-stream static pressure at model, lb/sq ft

$p_o$ standard sea-level static pressure, lb/sq ft

$p_l$ pressure measured by static orifice on afterbody, lb/sq ft

$\frac{\Delta p}{q} = \frac{p_l - p}{q}$ pressure coefficient

q dynamic pressure, lb/sq ft

R Reynolds number based on wing $\bar{c}$

S total wing area (including area enclosed within fuselage), sq ft

V velocity, ft/sec

W weight of model, lb

x distance between center of gravity and nose normal accelerometers, ft

$x_{ac}$ distance of aerodynamic center from leading edge of $\bar{c}$, percent $\bar{c}$

y distance from fuselage center line in spanwise direction, ft

$\alpha$ angle of attack, deg

$\beta$ angle of sideslip, deg

[redacted]

$\delta$ horizontal-tail incidence (in free-stream direction, referenced to wing plane, + trailing edge down), deg

$\theta/l$ influence coefficient, radians/lb (minus sign indicates twist in direction to decrease load)

$\ddot{\theta}$ angular acceleration in pitch, radians/sec$^2$

$\dot{\varphi}$ roll rate, radians/sec

$\dot{\psi}$ yawing velocity, radians/sec

The symbols $\alpha$, $\beta$, $\dot{\alpha}$, and $\dot{\theta}$ used as subscripts indicate the derivative of the quantity with respect to this subscript.

## MODEL AND INSTRUMENTATION

### Model

A sketch and photograph of the model are shown in figures 1 and 2, respectively. As shown, this model had a modified delta wing (arrow wing) with a 55° swept leading edge and an NACA 65A003 airfoil section. The rather slender, flat-sided fuselage had an effective fineness ratio of about 15 $\left(\text{where effective fineness ratio is the equivalent of } \frac{\text{Length of fuselage}}{D}\right)$ and mounted swept vertical and horizontal tails. The model as tested had only one horizontal-tail panel, as noted later in the text. The wing and horizontal tail were constructed of solid duralumin, the fuselage of magnesium castings and duralumin, and the vertical tail was made of magnesium. The wing flexibility was measured prior to flight and the wing structural influence coefficients measured with loads along the 50-percent-chord line are presented in figure 3.

The model was equipped with a 6-inch ABL Deacon rocket motor. As shown (fig. 1) this rocket was equipped with a "blast tube" extension. The reason for this extension will be discussed later in the text. At the exit of the rocket nozzle (i.e., at the joint between the nozzle and the blast tube) the ratio of jet static pressure to free-stream static pressure varied between 2.5 and 3.4, while the ratio of rocket-chamber pressure over free-stream static pressure varied between 75 and 100 as the model accelerated from $M \approx 1.2$ to $M \approx 2.3$. The jet Mach number at this joint was about 2.8 and the ratio of specific heats of the rocket gas was about 1.25. The exit area of the blast tube over exit area of the rocket nozzle was approximately 1.15.

[redacted]

Before the sustainer rocket was fired the model weight was 401 pounds, the center of gravity was at 25.4 percent $\bar{c}$ and 2.5 inches above the thrust line, and the moments of inertia in pitch, yaw, and roll were 111.8, 114.2, and 3.94 slug-ft$^2$, respectively. After sustainer rocket burnout the weight was 304 pounds, the center of gravity was at 24.3 percent $\bar{c}$ and 3.25 inches above thrust line and the moments of inertia in pitch, yaw, and roll were 101.9, 104.1, and 3.67 slug-ft$^2$, respectively.

## Instrumentation

Model instrumentation consisted of a telemeter transmitting continuous measurements of normal, transverse, and longitudinal accelerations near the center of gravity, normal acceleration of the nose, roll rate, angles of attack and sideslip, an afterbody static pressure, total head pressure, and horizontal-tail position.

Free-stream static pressure was determined through the use of data obtained from an NACA modified SCR-584 tracking radar and radiosonde and velocity over the first portion (0.5 to 13.5 seconds after launching) of the flight was checked by CW Doppler radar.

## TEST

The flight was conducted at the Langley Pilotless Aircraft Research Station at Wallops Island, Va. The model was accelerated to a Mach number of about 1.25 by a double underslung booster with two 6-inch ABL Deacon rocket motors. The model and booster combination is shown on the launcher in figure 2. After model-booster separation the model coasted for approximately 1 second and then the aforementioned sustainer rocket accelerated the model to a peak Mach number of 2.35.

Except for information on thrust and jet effects the data presented were obtained during coasting flight, following sustainer rocket burnout, as the model responded to the square-wave variation of horizontal-tail incidence. The tail settings used were approximately $-2^\circ$ and $-8^\circ$ in respect to the wing plane. The Mach number and dynamic pressure information on the model flight was obtained through use of the telemetered total head pressure data and the free-stream static-pressure data. The variation of test Reynolds number and static pressure with Mach number is shown in figure 4.

The right tail panel was knocked off by contact with the booster at model-booster separation. This became quite evident after examination of the telemeter records of the flight and tracking camera films. The

internal electrohydraulic pulsing mechanism was not damaged, however, and the left panel incidence was varied in a square-wave pattern throughout the coasting part of the test. Since there was only one tail panel operating, the model received considerable roll as well as pitch disturbance each time the tail pulsed.

## ANALYSIS

Because of the loss of one tail panel the model was subject to considerable lateral as well as longitudinal disturbance each time the tail incidence was changed. This is evident in the time histories shown in figure 5. As in tests of references 3 and 4 considerable coupling existed between the longitudinal and lateral modes. This coupling is especially evident when the tail is in the $-8^\circ$ position or when the trim roll rate is highest. Because of the considerable contributions of the motions in the lateral mode to the total resulting motion of the model the often-used two-degree-of-freedom-type analysis of reference 1 was invalid for obtaining $C_{m_\alpha}$ and $C_{m_q} + C_{m_{\dot{\alpha}}}$.

As in the case of the model of reference 3, the total lift, drag, and side-force information could be obtained more or less directly from accelerometers near the center of gravity and the $\alpha$ and $\beta$ indicator.

The nose and center-of-gravity normal accelerometers were used as in reference 3 to obtain $\ddot{\theta} - \dot{\varphi}\dot{\psi}$ by the following relationship:

$$\ddot{\theta} - \dot{\varphi}\dot{\psi} = \frac{g}{x}\left(A_{N_n} - A_{N_{cg}}\right)$$

The roll rate $\dot{\varphi}$ was measured directly and up to 14.6 seconds it was possible to obtain $\dot{\psi}$ from the tranverse accelerometer and side-slip data. The pitch acceleration $\ddot{\theta}$ could then be obtained from the above expression and the total pitching-moment coefficient was obtained from the following relationship:

$$C_m = \frac{1}{qSc}\left[I_Y\ddot{\theta} + \left(I_X - I_Z\right)\dot{\varphi}\dot{\psi} - I_{XZ}\left(\dot{\psi}^2 - \dot{\varphi}^2\right)\right]$$

After 14.6 seconds the telemeter channel reporting $\beta$ was inoperative and the pitching moment was obtained from

$$C_m = \frac{1}{qSc}\left[I_Y(\ddot{\theta} - \dot{\varphi}\dot{\psi}) + I_{XZ}\dot{\varphi}^2\right]$$

With the exception that the $I_{XZ}\dot{\varphi}^2$ term could be retained in the present analysis this method is similar to the simplification used in reference 3 and as in the case of that test was found to be entirely adequate for obtaining $C_m$. The values of $C_m$ include not only $C_m$ due to $\alpha$ but $C_m$ due to the rotary damping ($C_m$ due to $\dot{\theta}$ and $\dot{\alpha}$) and $C_m$ due to $\beta$, etc. As in the case of reference 3 the contribution of all these terms is believed to be small and to have no measurable effect on slopes, $\frac{dC_m}{dC_L}$, obtained through use of this method.

## Corrections

The angle of attack and sideslip at the center of gravity were obtained by correcting the instrument readings at the nose by the method given in reference 5.

Corrections were made for the effects of angular velocities and accelerations on some of the accelerometers displaced slightly (of the order of 4 inches and less) in longitudinal, vertical, and transverse directions from the center of gravity of the model. Such corrections were generally less than 2 percent of full-scale instrument range.

## Accuracy

On the basis of calculations similar to those described in the accuracy section of reference 3, the accuracies of the derivatives (as dependent on basic instrument accuracies) are believed to be at least as good as follows:

| At M | Accuracy in percent of quantity | | | | |
|---|---|---|---|---|---|
| | $C_{L_\alpha}$ | $x_{ac}$ | $C_{D_{min}}$ | $\Delta\alpha_{trim}$ | $\Delta C_{L_{trim}}$ |
| 2.1 | 3 | 3 | 5 | 2 | 3 |
| 1.6 | 4 | 5 | 10 | 2 | 4 |
| 1.1 | 5 | 5 | 25 | 2 | 7 |

## RESULTS AND DISCUSSION

Basic data.- Most of the basic information obtained from this test is given in figures 5, 6, 7, 8, and 9. These figures show time histories and plots of $C_L$ against $\alpha$, $C_m$ against $C_L$, $C_D$ against $C_L$, and $C_Y$ against $\beta$, respectively. There seems to be no strong evidence of aerodynamic coupling terms such as $C_{m_\beta}$ or $C_{L_\beta}$ in the pitching moment or lift cross plots. It is believed these would be apparent, if they were present, because of the relative amplitude and frequencies of $\alpha$ and $\beta$.

Longitudinal trim.- Variation of trim angle of attack and lift coefficient with Mach number are shown in figure 10. The solid lines shown represent the mean line through the oscillations and the points were obtained from plots of $C_L$ against $\alpha$ and/or $C_m$ against $C_L$ (figs. 6 and 7, respectively). As shown, the trim angle of attack for a given tail setting increased with increasing Mach number, whereas the trim lift was approximately constant.

The power-on trim curves are also included in this figure and show that coincidentally the power effect on trim was about the same as changing the tail setting from $\delta = -2^\circ$ to $\delta = -8^\circ$. Of course, the change in trim resulting from change in tail setting would have been approximately twice that shown if both horizontal-tail panels had been on the model. The power effects will be discussed in more detail later in this text.

Lift and stability.- The lift-curve slopes obtained from plots of figure 6 are shown plotted against Mach number in figure 11. There seems to be no consistently large effect of trim angle of attack (different tail settings) on the lift-curve slope. The theoretical lift-curve slope for the rigid configuration was obtained through theoretical methods outlined in reference 6 and was corrected for flexibility effects of the wing through use of the influence coefficients shown in figure 3 and the procedure outlined in the appendix of reference 2. The agreement between theory and data is extremely good.

The aerodynamic-center information obtained from slopes of figure 7 and the center-of-gravity location is given in figure 12, along with theoretical information obtained through use of references 6 and 2. Here again agreement between theory and test data is generally very good.

The theoretical information on $C_{L_\alpha}$ and $x_{ac}$ is for a model with one horizontal tail, that is, as tested. The contribution of one tail panel to lift was very small (estimated to be about 2 percent of

total $C_{L_\alpha}$) and the contribution to $x_{ac}$ was estimated to be about 5 percent $\bar{c}$ at M = 2.1 and 2 percent $\bar{c}$ at M = 1.1.

Drag.- Because of the rather small amplitude of the pitch oscillations, drag information on this configuration is somewhat limited. However, drag at low lift coefficients was obtained from the plots of figure 8 and from the time histories (not shown) and is given in figure 13. Drag data are not presented below a Mach number of about 1.6 because, as indicated in the accuracy table, the error in $C_D$ may be in excess of 10 percent.

Lateral force.- The variation of the lateral-force parameter $C_{Y_\beta}$ with Mach number is shown in figure 14 as obtained from plots of figure 9. Also included is a theoretical estimate of the vertical-tail contribution obtained through use of reference 6 and approximately corrected for a small flexibility effect. The difference in the estimated tail contribution and the total $C_{Y_\beta}$ indicates that the exposed vertical tail contributes roughly 60 percent of total lateral force. This seems reasonable in view of the relatively large ratio of fuselage side area over vertical-tail area.

Thrust and jet effects.- In the tests of reference 7 it was found that on a configuration like the one reported herein, but without the blast tube extension (see sketches on fig. 15), there were very strong jet-induced effects on the longitudinal trim. The model of reference 7 had a rocket with ratio of total pressure to free-stream static pressure of approximately 100, ratio of jet exit static pressure to free-stream static pressure of approximately 4.4, jet exit Mach number of about 2.6, and ratio of specific heats of rocket gas of 1.22. It was evident that if the rocket in the model of reference 7 had thrusted for as long a time as the rocket used in the present test that model would have diverged in its lateral motion, perhaps to the point of destruction. It was felt that lateral dynamic instability of that model resulted from its being trimmed at a negative angle of attack during power-on, which was caused by jet-induced effects on air flow at the tail. The blast tube was therefore added to the present model in an effort to eliminate or at least reduce this effect.

Shown in figure 15 are the total change in $C_{N_{trim}}$ due to the power effect, the portion calculated due to the thrust line being below the center of gravity and the remaining portion, which is the part of trim change due to the jet-induced effect. The portion of $\Delta C_{N_{trim}}$ attributable to thrust misalinement was calculated from the vertical center-of-gravity data (the vertical center-of-gravity location was assumed to vary

linearly with time as the rocket grain burned) and thrust characteristics determined through use of thrust stand data obtained on other Deacon rockets. Also shown in figure 15 is the net jet-induced effect on $\Delta C_{N_{trim}}$ of the model of reference 7 (without blast tube). The model without a blast tube had two horizontal tail panels, but the jet-induced effect on trim of this same configuration with only one tail panel would probably be at least one-half that indicated on the figure.

The net jet-induced effect on $C_{N_{trim}}$ of the present model is extremely small as compared to this effect on the model of reference 7 and even though there are other differences in configuration, that is, one instead of two tail panels and somewhat different basic rocket characteristics, the major difference is believed attributable to the addition of the blast tube. The presence of the blast tube probably changed the induced effect by a combination of straightening the jet flow, changing the exit pressure ratios (through a slight expansion and through some internal shock losses), and most important, by releasing the jet further downstream.

An orifice to measure a static pressure in the vicinity of the afterbody (see sketch in fig. 16) affected by jet effects was installed on the model of the present test. Data obtained from this measurement are shown in figure 16 in the form of the variation of $\Delta p/q$ with Mach number for power on and off. As shown, the total power effect (combined effect of changes in angle of attack and pressure field) increased the static pressure from a value considerably less than to a value higher than free-stream static pressure. This increase is believed to be mainly due to the jet causing a turning of the external flow as discussed in reference 7, since the power-off curve was obtained over a range of angle of attack (two different $\delta$ values) and appeared to be comparatively invariant with changes in $\alpha$ alone.

The jet effect on the pressure at this particular orifice location was such as to produce a small negative $\Delta C_{N_{trim}}$ (the order of -0.02 if uniform pressure distribution assumed downstream of orifice) which, of course, is opposite to the small jet-induced effect shown in figure 15. This apparent discrepancy may be due to the presence of a counteracting jet-induced pressure field acting in the opposite direction or perhaps due in part to lack of precision in obtaining the small net effect shown in figure 15.

To summarize the jet-effects information, it appears that the addition of a blast tube almost entirely eliminated jet-induced effects on trim; and examination of the time history (fig. 5) during power-on indicates that the lateral dynamic instability experienced in tests of reference 7 was also alleviated.

[redacted]

## CONCLUDING REMARKS

A rocket-propelled model of an airplane configuration having an arrow wing with 55° leading-edge sweep and a flat-sided fuselage mounting swept horizontal and vertical tails has been tested through use of the pulsed-control technique at Mach numbers between 1.0 and 2.3.

The results of this test indicate good agreement between measured lift and stability data and corresponding theoretical estimates and indicate that the addition of a blast tube reduced trim changes which resulted from jet-induced flow effects at the tail.

Langley Aeronautical Laboratory,
National Advisory Committee for Aeronautics,
Langley Field, Va., December 7, 1955.

REFERENCES

1. Gillis, Clarence L., Peck, Robert F., and Vitale, A. James: Preliminary Results From a Free-Flight Investigation at Transonic and Supersonic Speeds of the Longitudinal Stability and Control Characteristics of an Airplane Configuration With a Thin Straight Wing of Aspect Ratio 3. NACA RM L9K25a, 1950.

2. Vitale, A. James: Effects of Wing Elasticity on the Aerodynamic Characteristics of an Airplane Configuration Having 45° Sweptback Wings As Obtained From Free-Flight Rocket-Model Tests at Transonic Speeds. NACA RM L52L30, 1953.

3. Peck, Robert F., and Coltrane, Lucille C.: Longitudinal Characteristics at Transonic and Supersonic Speeds of a Rocket-Propelled Airplane Model Having a 60° Delta Wing and a Low Swept Horizontal Tail. NACA RM L55F27, 1955.

4. Parks, James H.: Experimental Evidence of Sustained Coupled Longitudinal and Lateral Oscillations From a Rocket-Propelled Model of a 35° Swept Wing Airplane Configuration. NACA RM L54D15, 1954.

5. Ikard, Wallace L.: An Air-Flow-Direction Pickup Suitable for Telemetering Use on Pilotless Aircraft. NACA RM L53K16, 1954.

6. Margolis, Kenneth, and Bobbitt, Percy J.: Theoretical Calculations of the Stability Derivatives at Supersonic Speeds for a High-Speed Airplane Configuration. NACA RM L53G17, 1953.

7. Peck, Robert F.: Jet Effects on Longitudinal Trim of an Airplane Configuration Measured at Mach Numbers Between 1.2 and 1.8. NACA RM L54J29a, 1955.

[redacted]

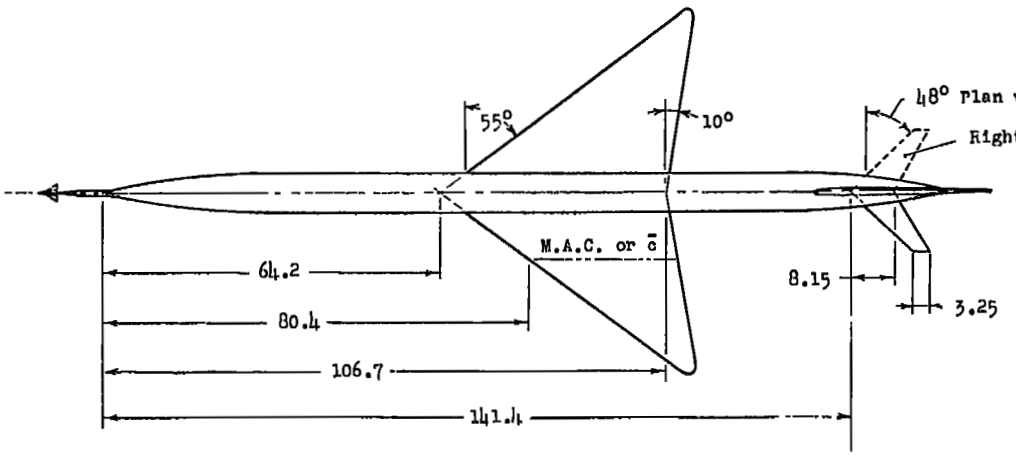


Wing
- Area (inc. fus.).....10.00 sq ft
- M.A.C. ..... 2.36 ft
- Aspect ratio ..... 3.20
- Airfoil .....65A003

Horizontal Tail (Plan View,Both panels)
- Area ..... 0.90 sq ft
- M.A.C. ..... .50 ft
- Aspect ratio ..... 4.00
- Airfoil .....65A003

Vertical Tail
- Area ..... 2.47 sq ft
- M.A.C. ..... 1.73 ft
- Aspect ratio ..... 2.03
- Airfoil .....65A005

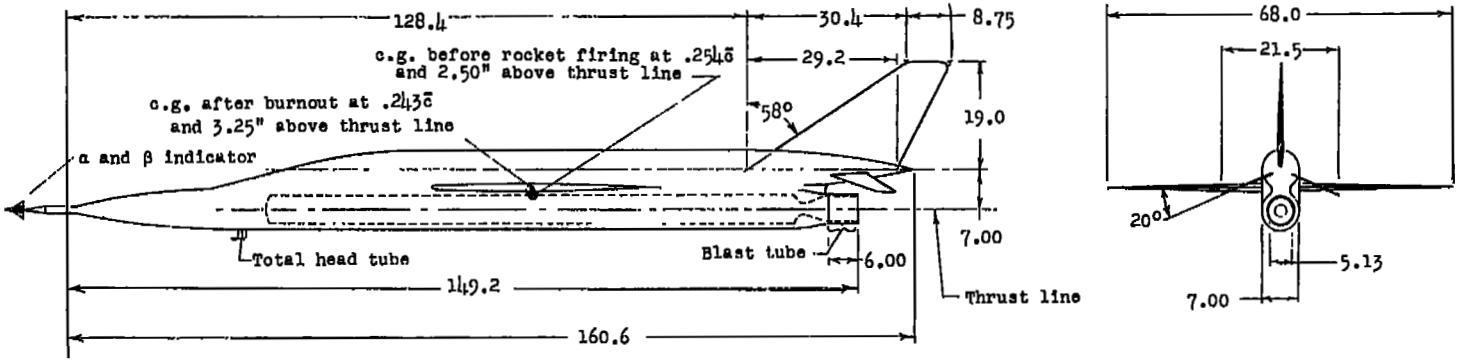


Figure 1.- Sketch of test configuration. Dimensions are in inches except as noted.

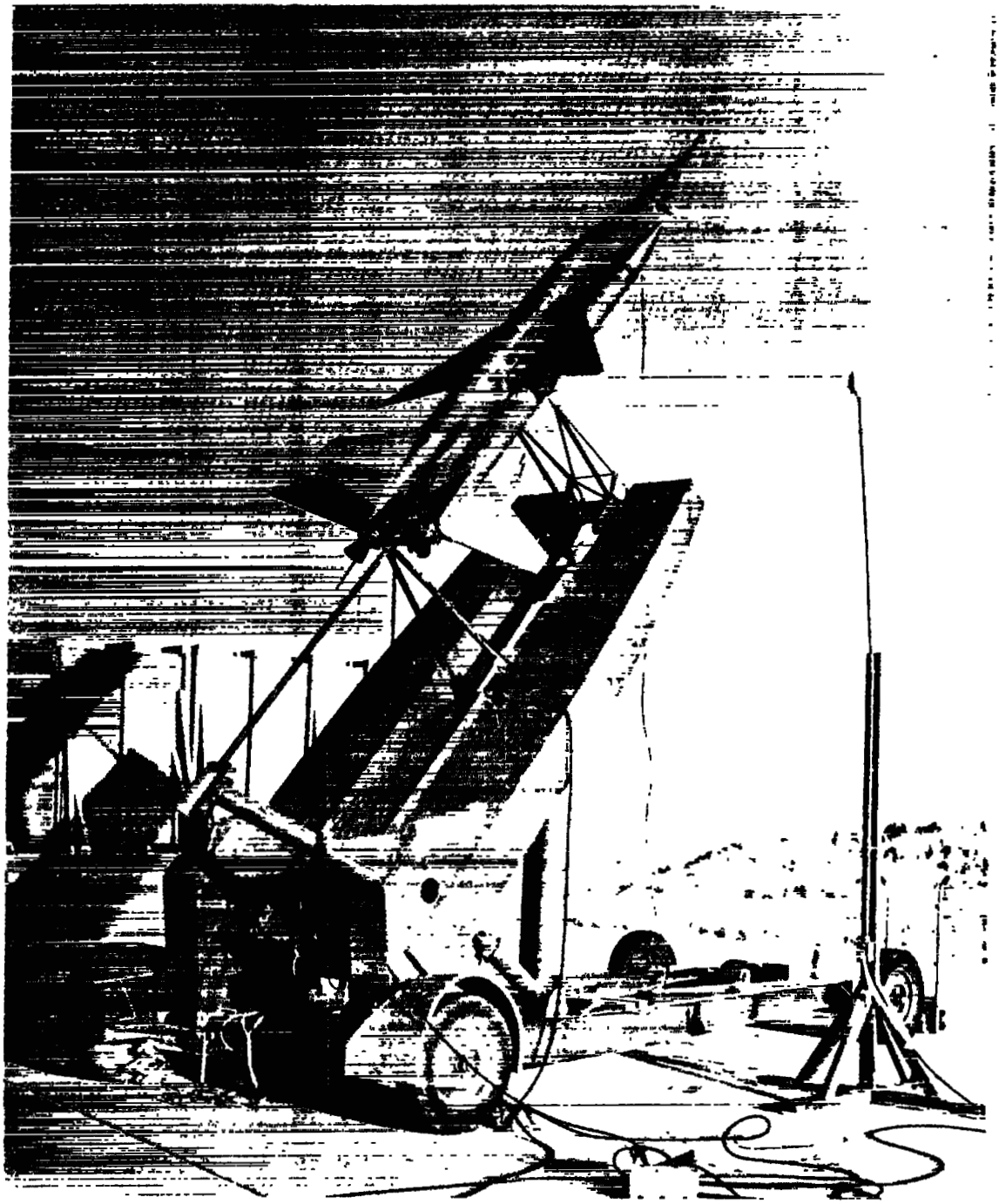

L-87265.1

Figure 2.- Model and booster on launcher.

[redacted]

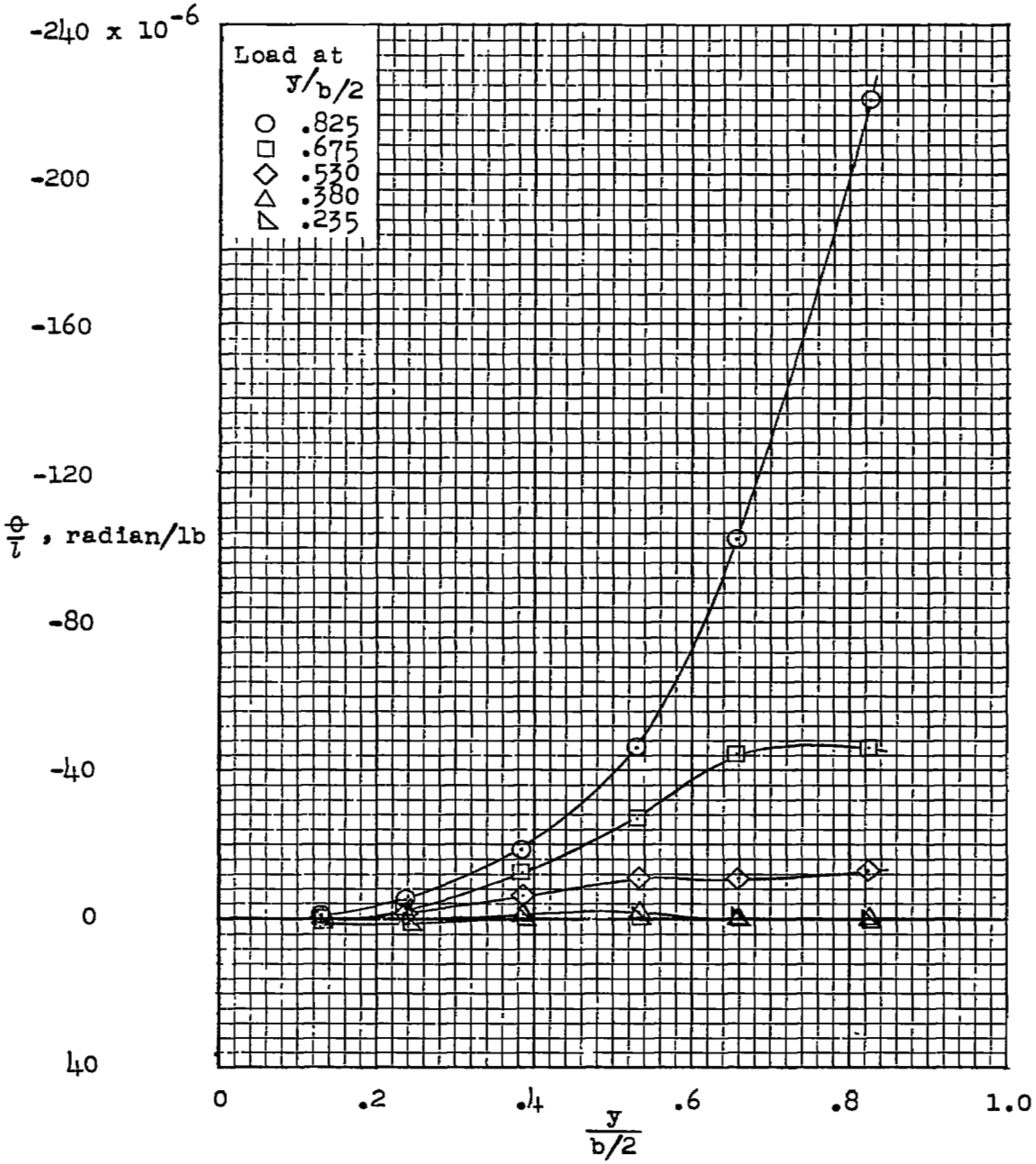


Figure 3.- Wing influence coefficients measured with loads along 50-percent chord line.

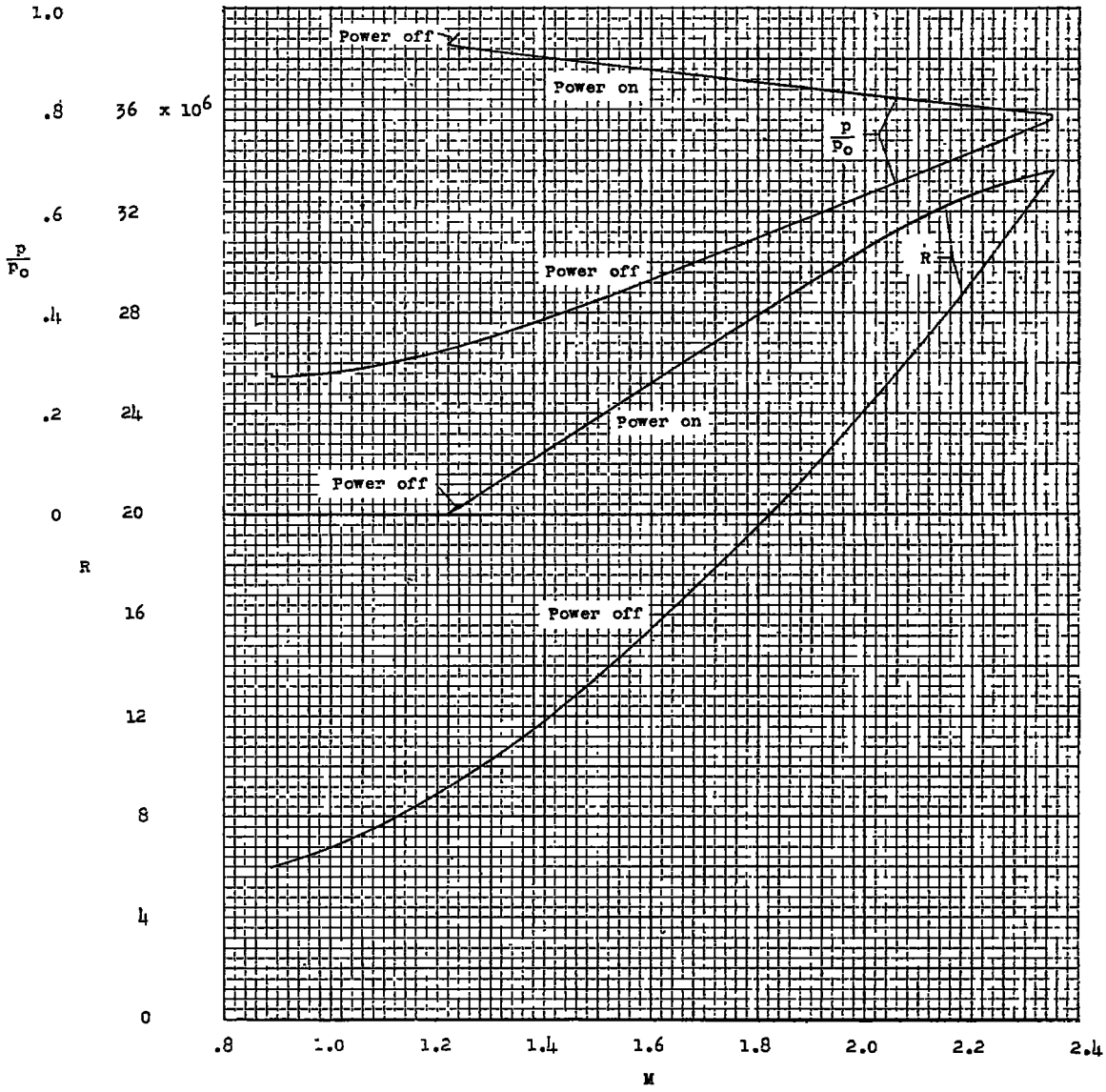


Figure 4.- Variation of test Reynolds number and static-pressure ratio with Mach number.

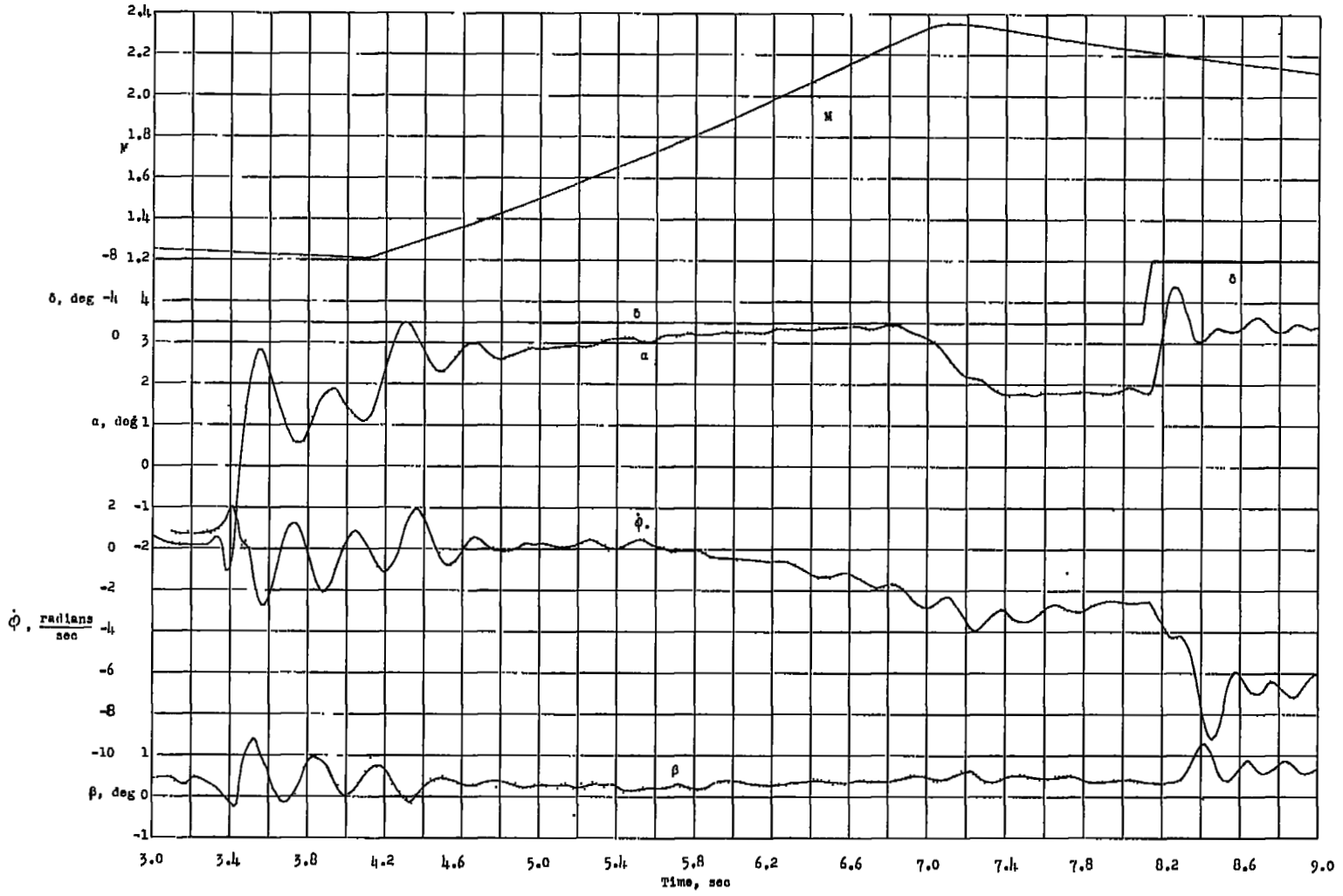


Figure 5.- Time history of Mach number, tail deflection, angle of attack, rate of roll, and angle of sideslip during first portion of flight.

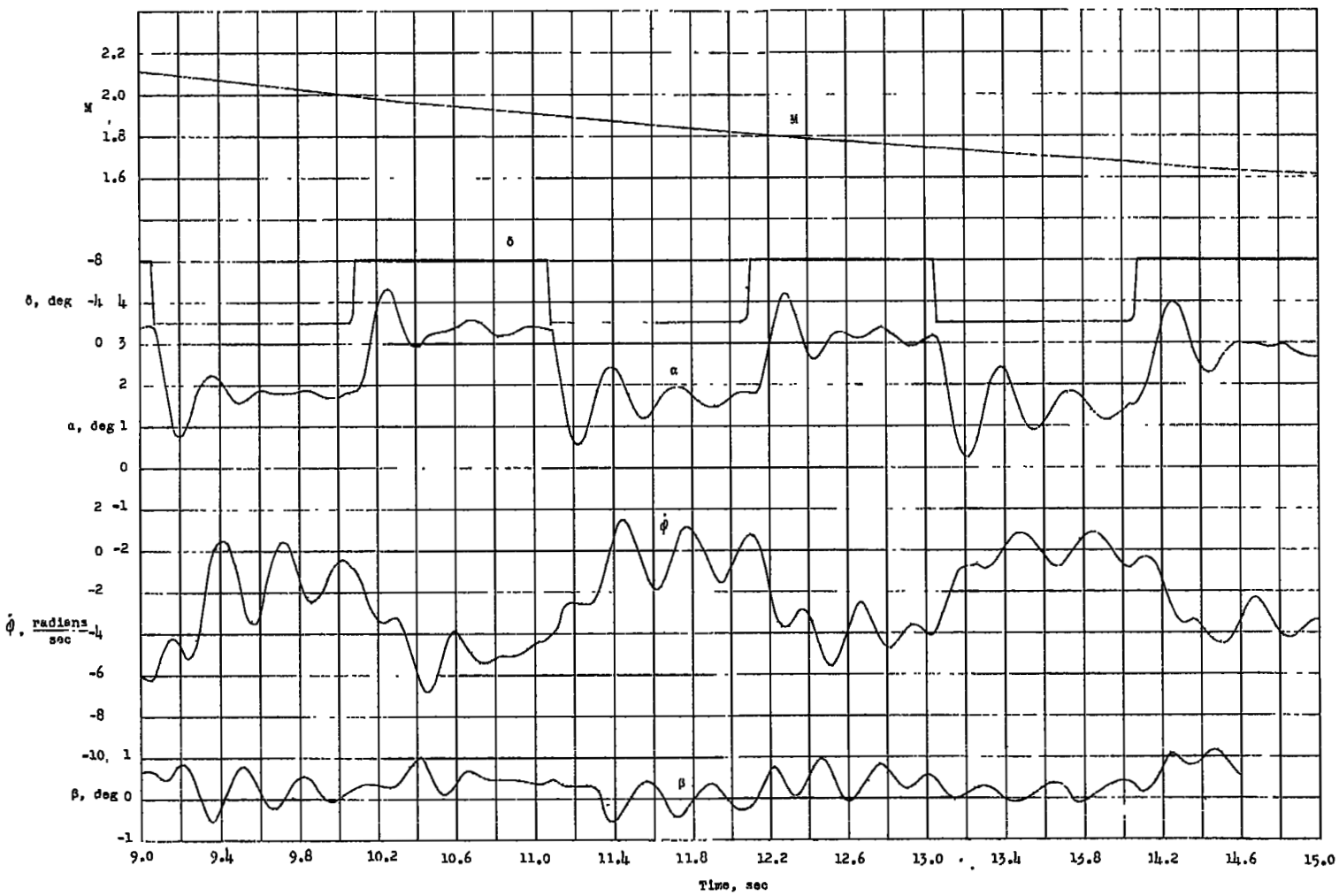


Figure 5.- Concluded.

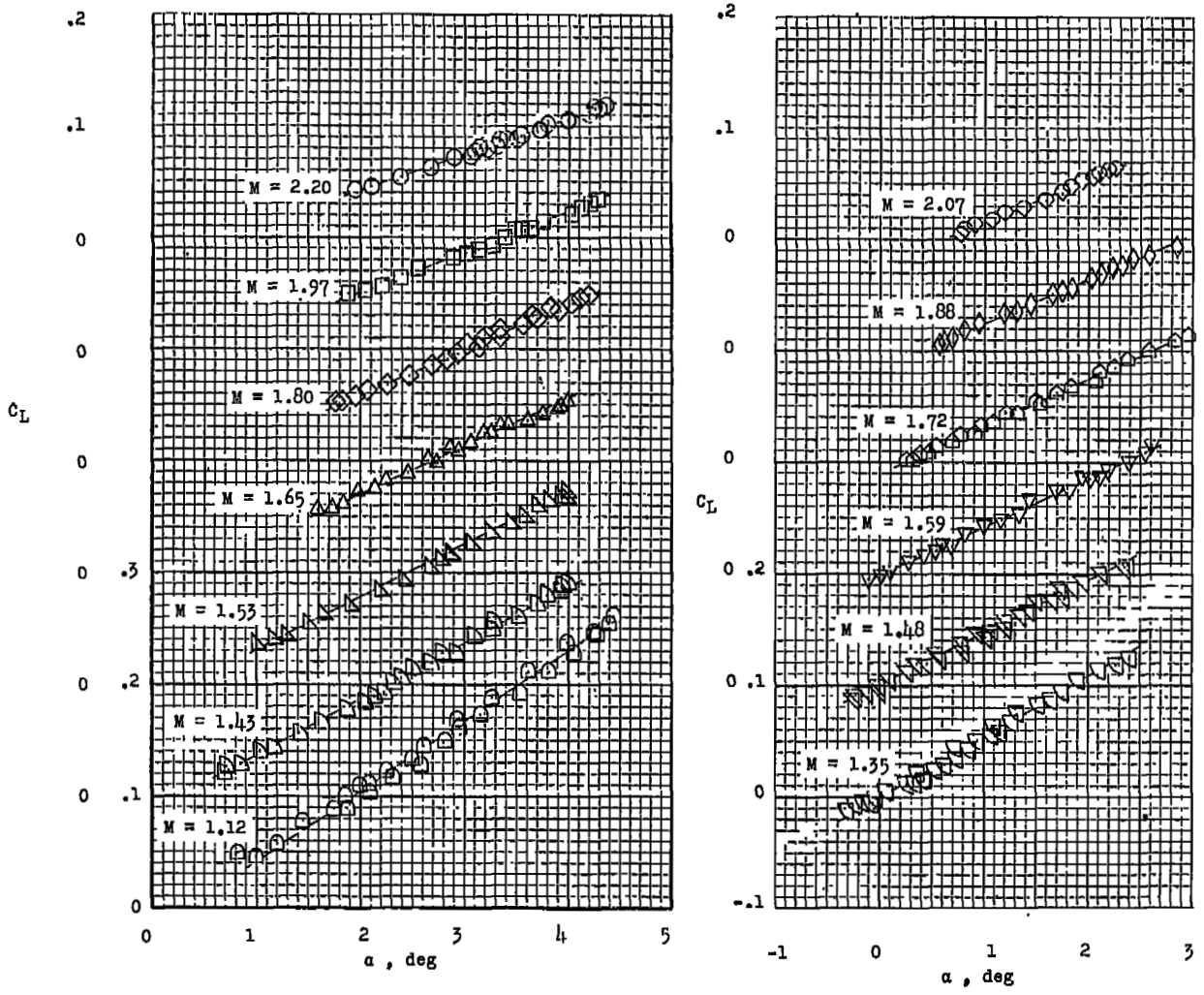


(a) $\delta = -8^{\circ}$. (b) $\delta = -2^{\circ}$.

Figure 6.- Variation of lift coefficient with angle of attack.

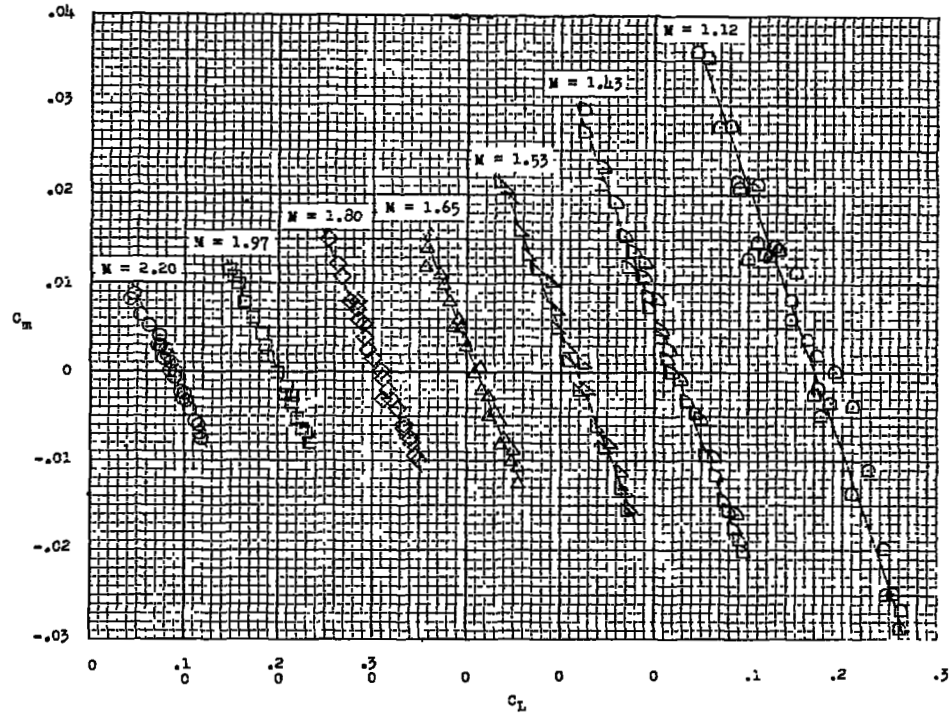


(a) $\delta = -8^\circ$.

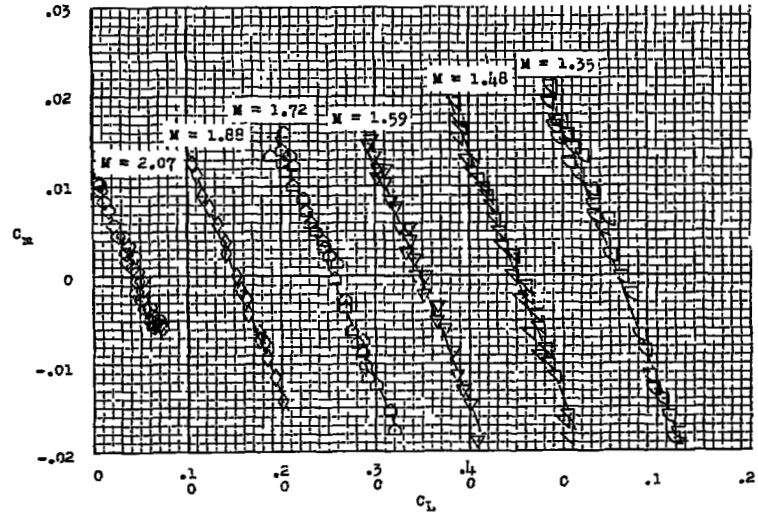


(b) $\delta = -2^\circ$.

Figure 7.- Variation of pitching-moment coefficient with lift coefficient for center of gravity at $0.243\bar{c}$.

[redacted]

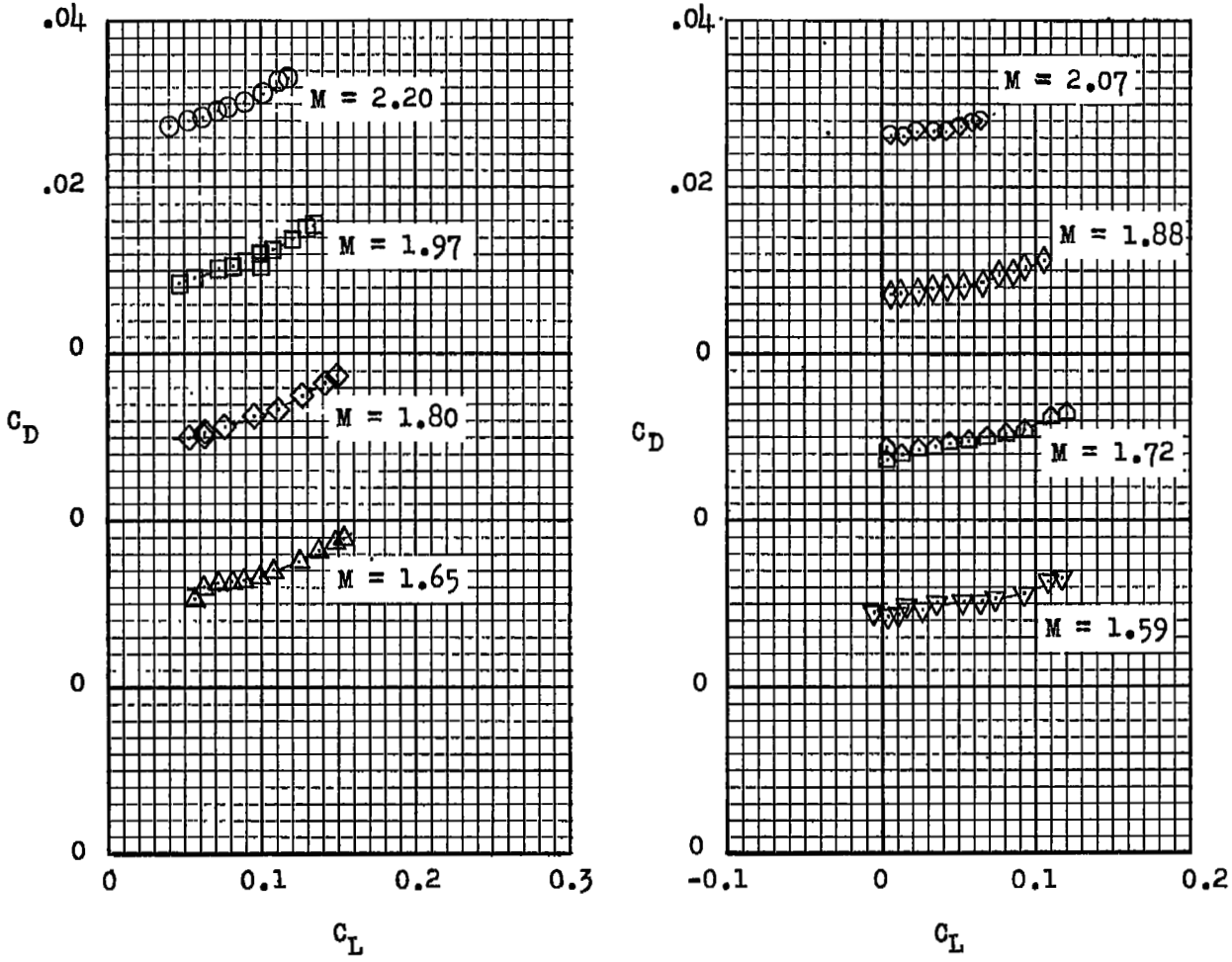


(a) $\delta = -8^\circ$.

(b) $\delta = -2^\circ$.

Figure 8.- Variation of drag coefficient with lift coefficient and Mach number.

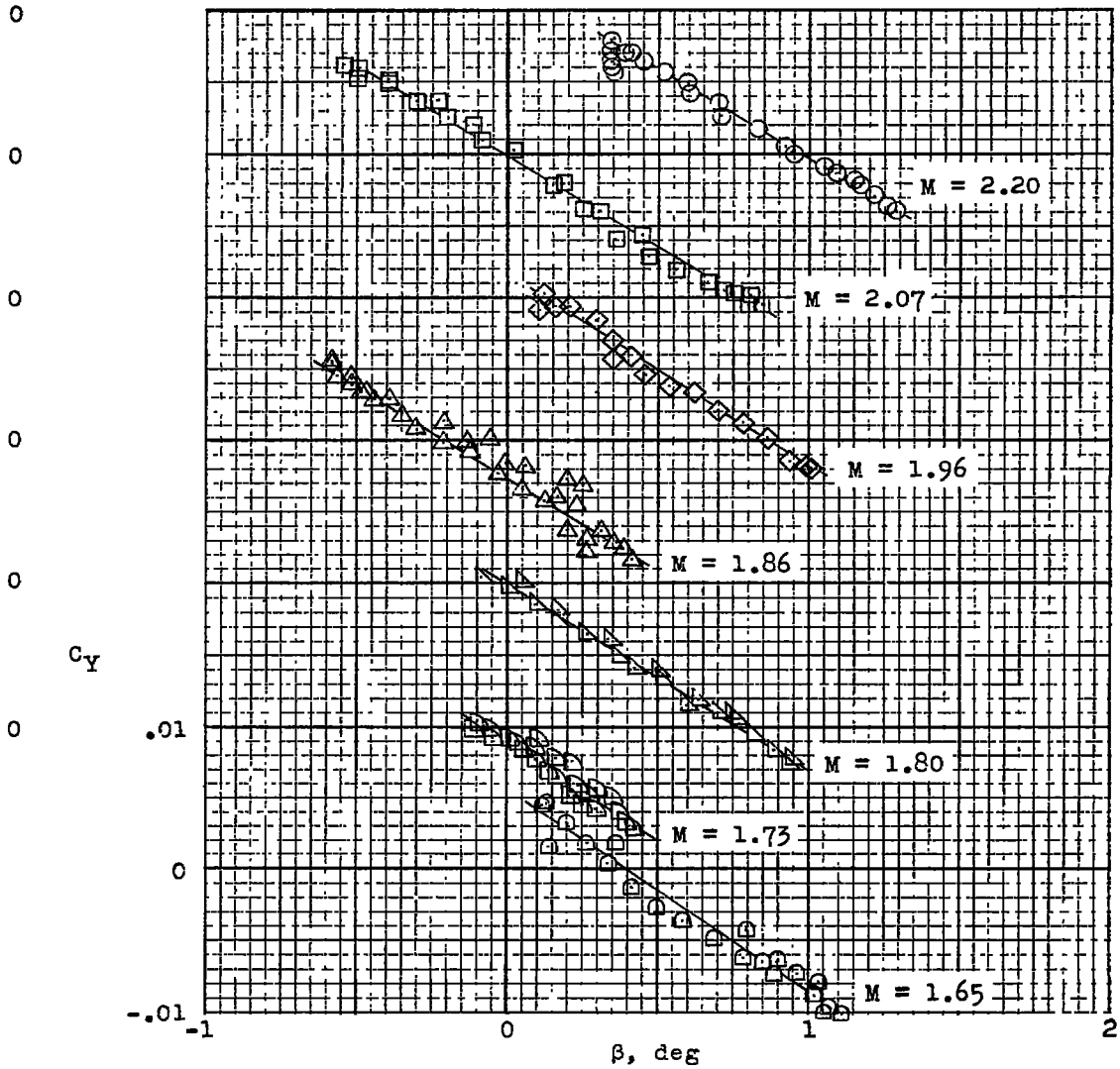


Figure 9.- Variation of lateral-force coefficient with angle of sideslip.

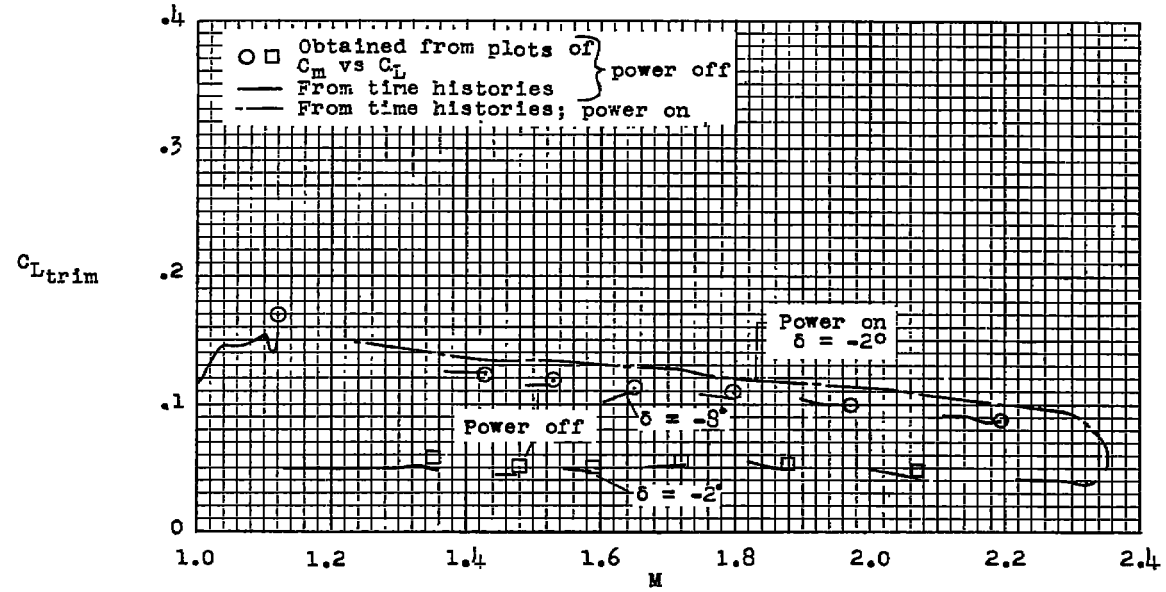


(a) Trim lift coefficient.

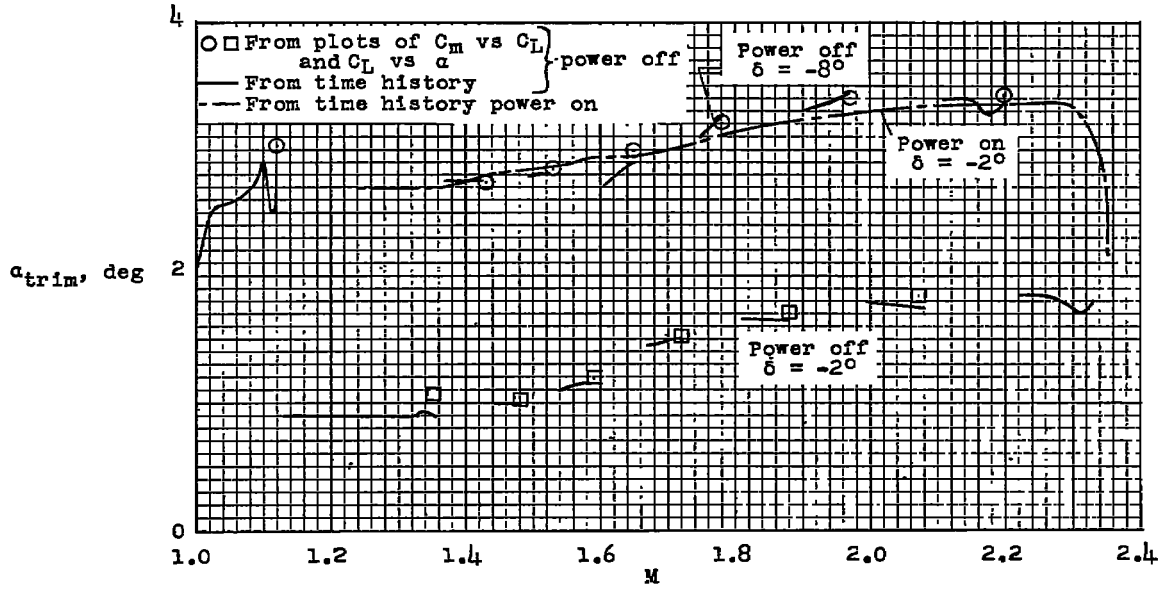


(b) Trim angle of attack.

Figure 10.- Variation of trim characteristics with Mach number for power on and off.

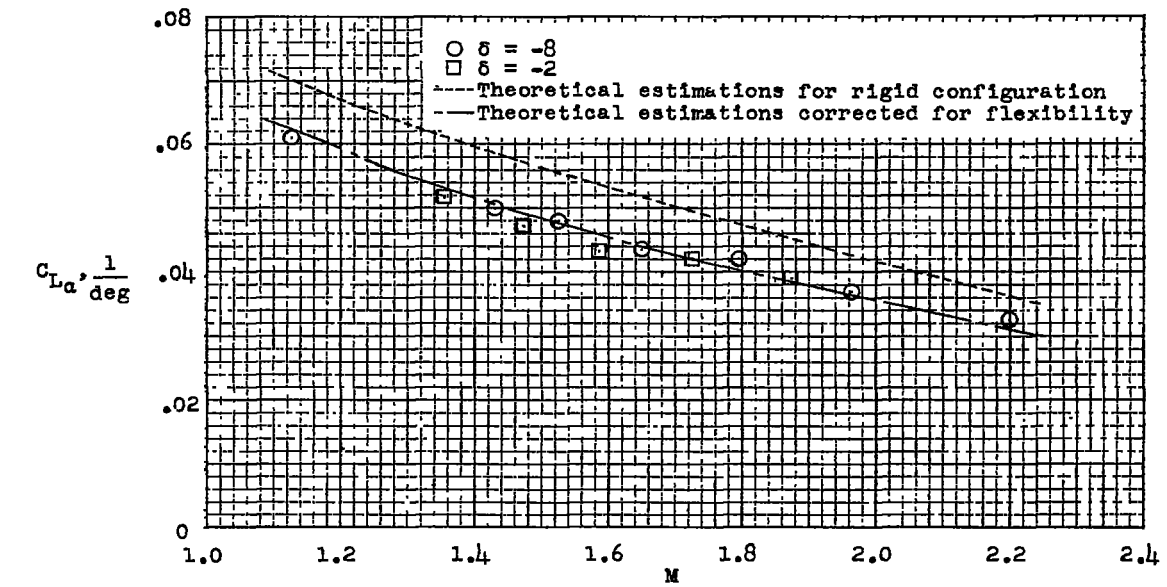


Figure 11.- Variation of lift-curve slope with Mach number.

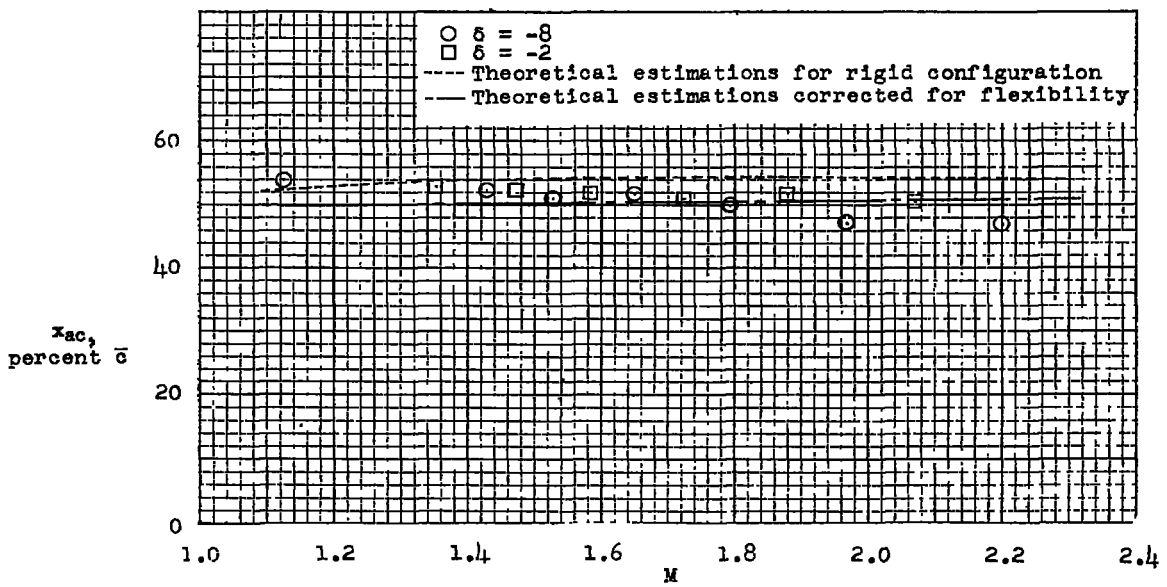


Figure 12.- Variation of aerodynamic-center location with Mach number.

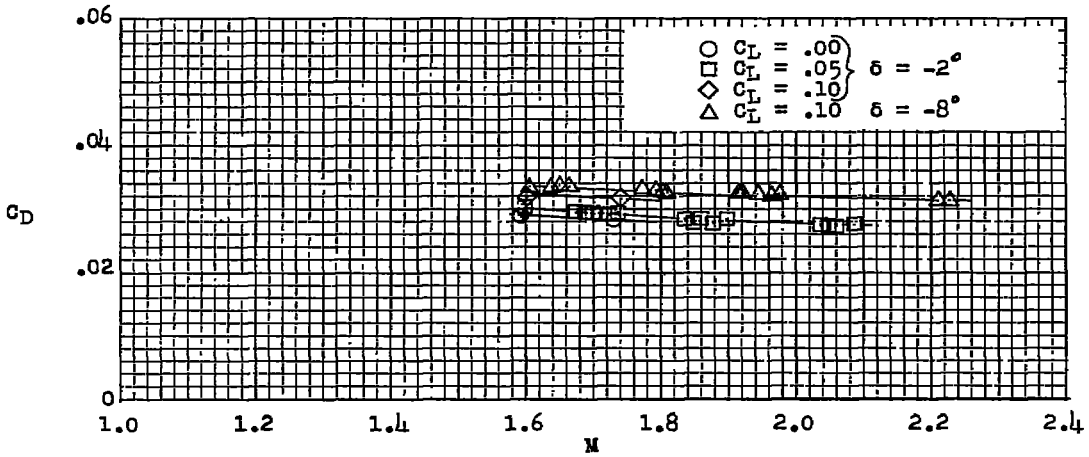


Figure 13.- Variation of drag coefficient with Mach number.

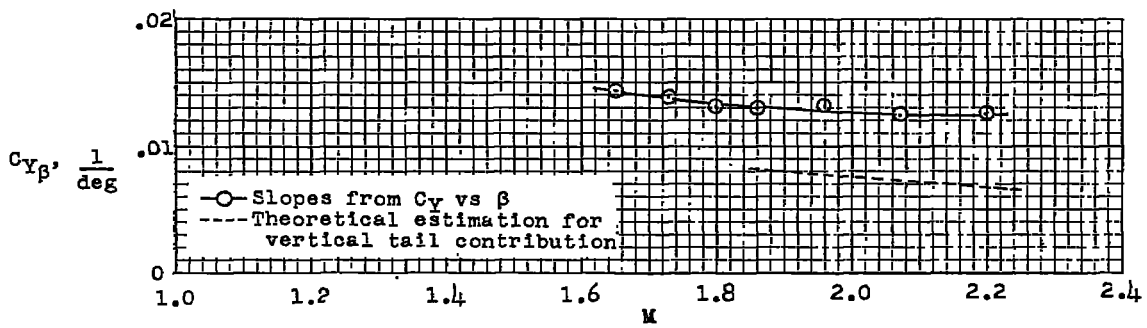


Figure 14.- Variation of $C_{Y_\beta}$ with Mach number.

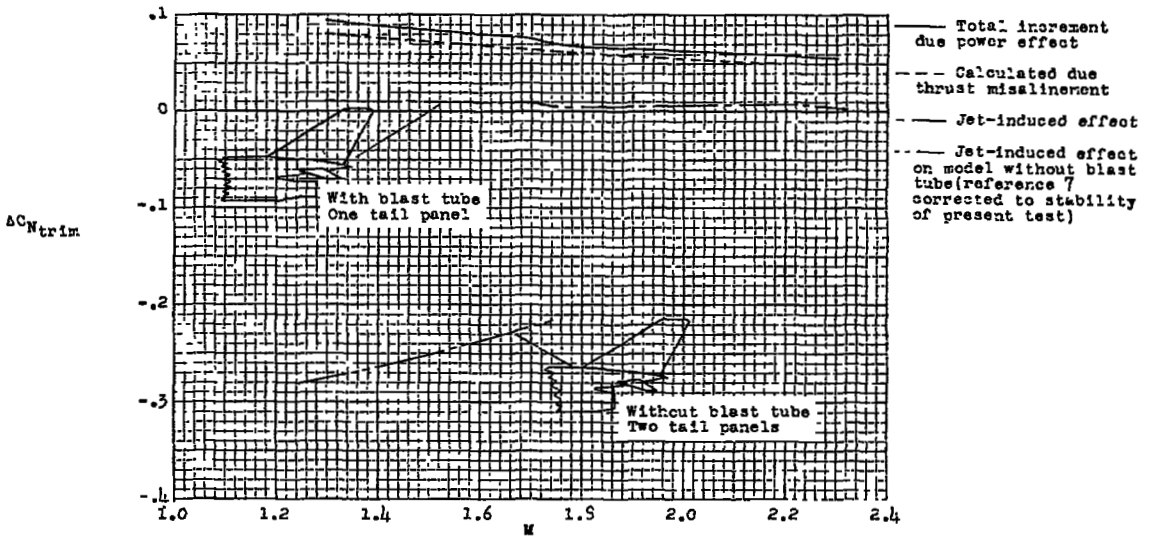


Figure 15.- Power effects on trim normal force.

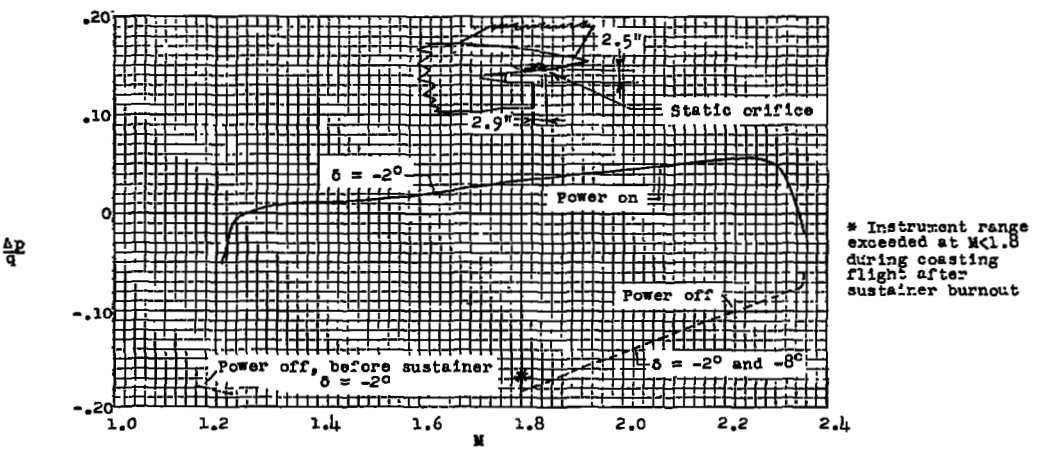


Figure 16.- Pressure coefficient measured at point on tail boom just off blast tube exit for power-on and power-off conditions.